## CHAPTER IV
RESULTS AND DISCUSSION

4.1 Monte Carlo Simulation

The results of the simulation of three different system geometries of scatterometer were compared in Figure 4.1, which shows the relationship between the scattered neutron flux obtained from the MCNP4C program and the actual void fraction. The density of the mixture was varied following Equation (3.1) in order to obtain different values of void fraction in the range from 0 to 1.
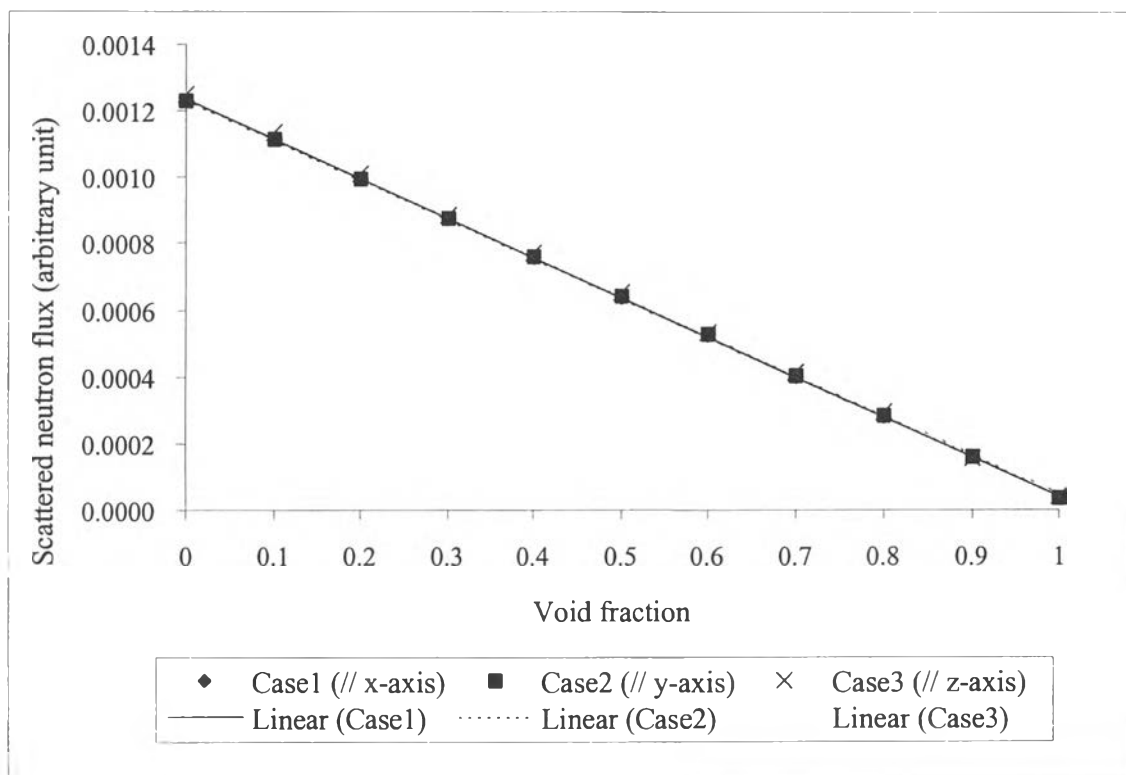
Figure 4.1 Comparison of the correlation between void fraction and the scattered neutron flux for steam-water mixture at 260°C for three different system geometries using the Monte Carlo method.

All three cases show the trend-as the void fraction decreases; the scattered neutron count rate increases. This was because the increase in the liquid fraction slows down neutrons more efficiently than the vapor phase because of the higher

concentration of hydrogen atoms. Consequently, the scattered neutrons were proportional to the liquid fraction.

Linearity was achieved over the entire range of void fraction for each case and its slope was nearly the same. This meant that it did not matter if the geometries of the scatterometer were arranged in different configurations as long as the detector was located perpendicular to both neutron beam and test section. Therefore, the technique of fast neutron scattering for a steam-water mixture was theoretically adequate for measuring the void fraction.

The example of the output file for case 1 is given in Appendix A and the raw data are summarized in Appendix C. As suggested in the program manual, the relative error for a point detector should be reliable when the value was less than 0.05. Therefore, each point was acceptable due to the small relative errors.
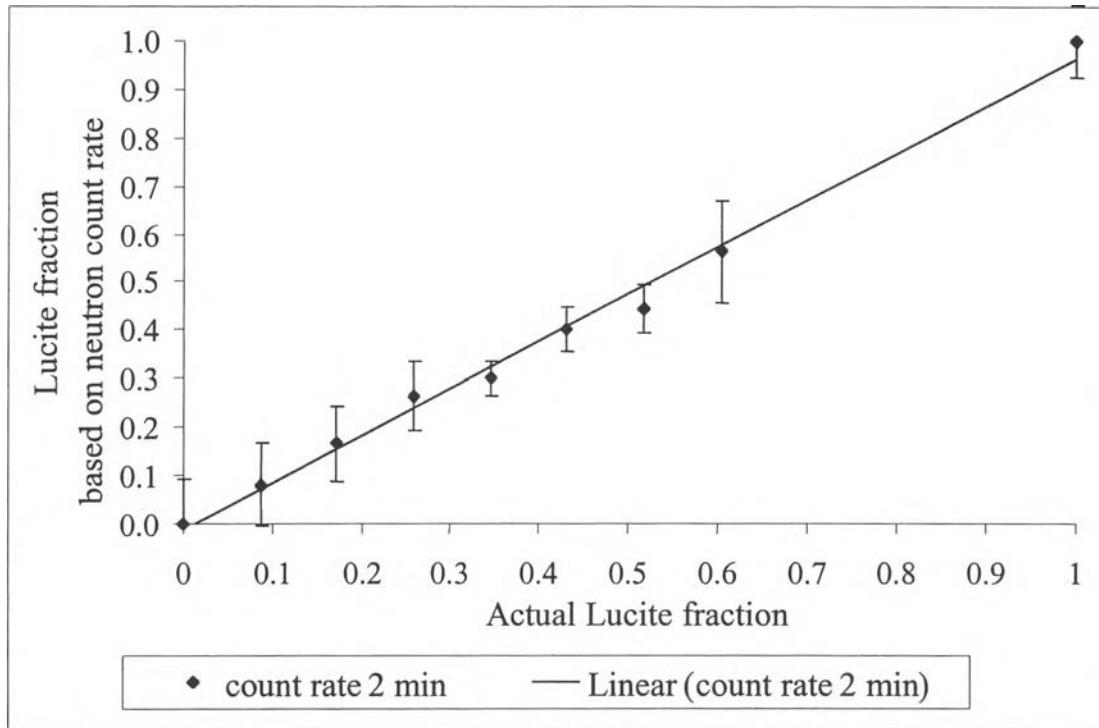
4.2 Static Air-Lucite Experiment

The correlation between neutron count rate and Lucite fraction was depicted in Figure 4.2. The raw data are shown in Appendix D. The mean neutron count rates for each Lucite fraction are shown in Table 4.1. As mentioned before, Lucite rods were used to simulate water; therefore, when the Lucite fraction increased, the neutron count rate also increased. This was because the total number of the hydrogen atom from the Lucite rod increased.

Table 4.1 Estimated Lucite fraction calculated from the mean of neutron count rate for various Lucite fraction.

Actual Lucite fraction	Mean count rate for 2 minutes	Estimated Lucite fraction
0	1460.10	0
0.086	1466.60	0.080
0.173	1472.30	0.166
0.259	1479.50	0.264
0.345	1482.20	0.300
0.432	1489.60	0.401
0.518	1492.70	0.443
0.604	1501.60	0.564
1.000	1533.70	1.000
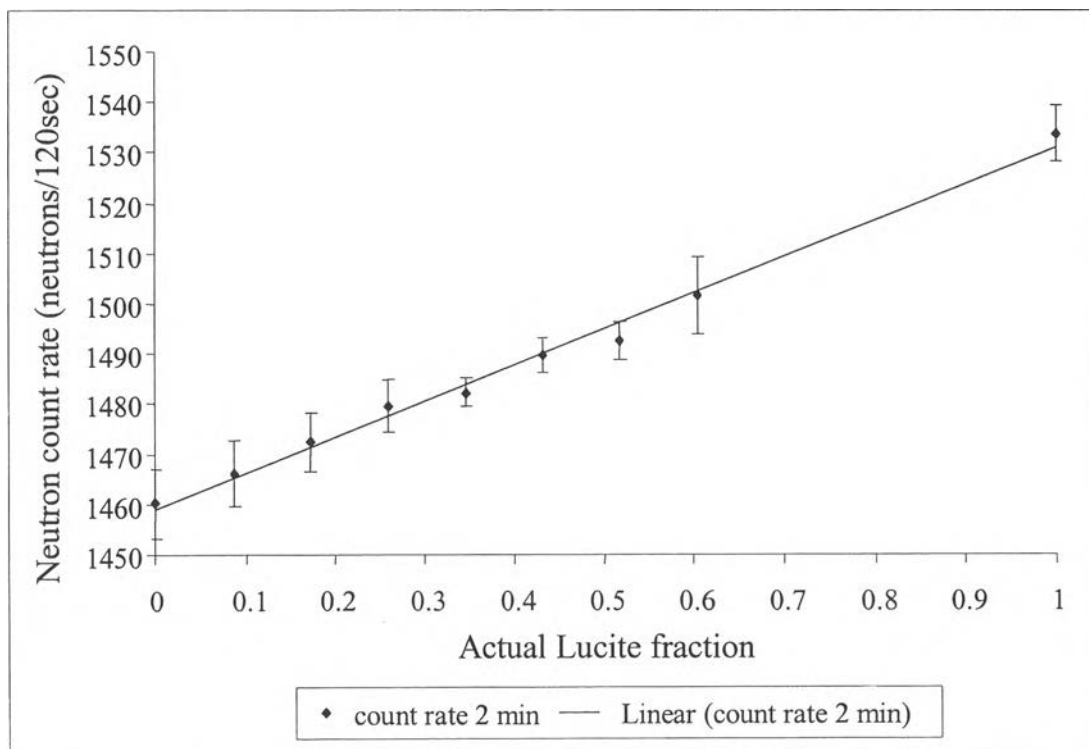
Figure 4.2 Correlation between neutron count rate and actual Lucite fraction at atmospheric conditions.

Figure 4.3 Correlation between Lucite fraction based on neutron count rate and actual Lucite fraction in the static air-Lucite experiment.

After applying Equation (2.1) to the neutron count rate for calibration, the estimated Lucite fractions shown in Table 4.1 were estimated. From Figure 4.3, the linear response was achieved between the estimated and known Lucite fraction. Thus, there was the possibility of predicting water fraction or void fraction by using this design of scatterometer. Therefore, the dynamic nitrogen-water experiment was continued.

4.3 Dynamic Nitrogen-Water Experiment

4.3.1 Fast Neutron Scattering Technique

The results from one size of screen and two sizes of filters, which were 0.6 cm, 15 μm and 60 μm, were compared as shown in Figures 4.4 and 4.5. The raw data are found in Appendix E.
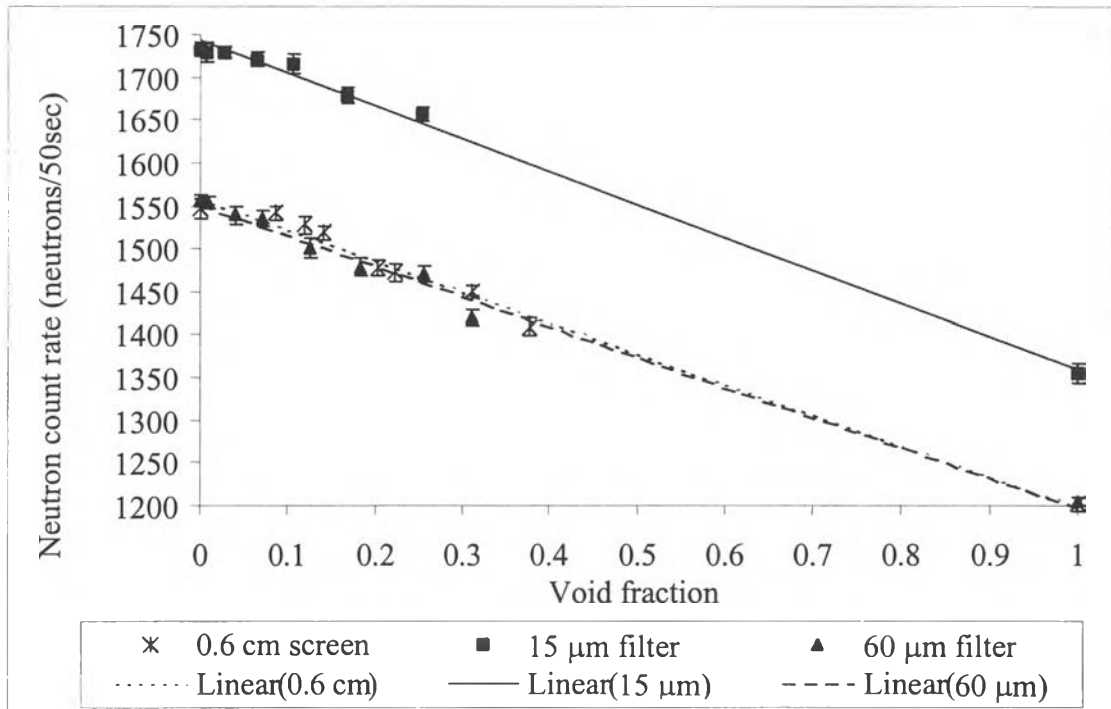
Figure 4.4 Comparison of the correlations between neutron count rate and the void fraction at atmospheric conditions for different bubble sizes.
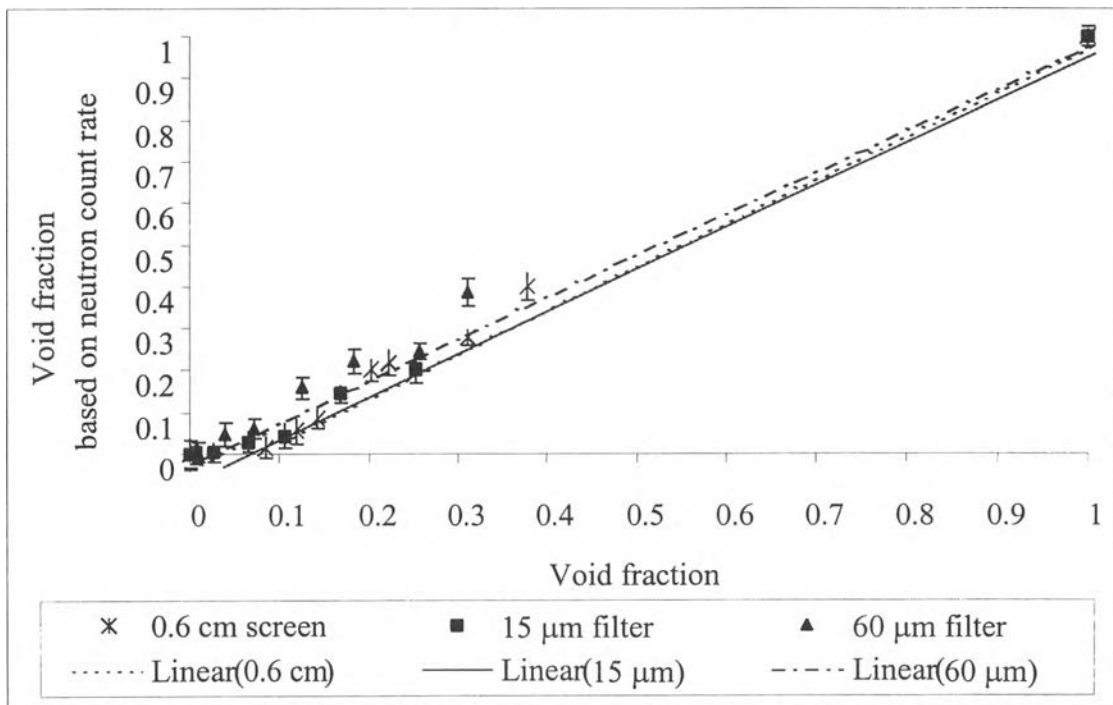

Figure 4.5 Comparison of the correlations between void fraction based on neutron count rate and void fraction at atmospheric conditions for different bubble sizes.

The void fraction was calculated from the rise of water at each nitrogen flow rate. Figure 4.4 shows that the fast neutron scattering technique had a good potential to be used in two-phase flow system for measuring the void fraction because every case gave linearity between the void fraction and neutron count rate. Moreover, the bubble sizes did not significantly affect the relationship between neutron count rate and void fraction since the slope of the line for each case was essentially the same. However, the neutron count rate for the 15 µm filter was different from the other two cases, presumably since it was impossible to obtain the same values of neutron count rate for each case due to inadvertent changes in the position of the scatterometer. A calibration process can eliminate this problem by applying equation (2.1) to the neutron count rate, as shown in Figure 4.5. Then, the linearity of the correlation between the void fraction based on neutron count and the void fraction was still obtained and the slopes of all cases were the same. Insensitivity to the change in the size of the bubble proved that there was no effect on the performance of the scatterometer.

4.3.2 Fast Neutron Transmission Technique

As a result of the previous part, an experiment on the fast neutron transmission techniques was only performed on the 15-µm filter; the result was shown in Figure 4.6. The trend between neutron count rate and void fraction from the transmission technique was the same as that from the scattering technique. This was not expected because, in the transmission technique, as the void fraction increases there was less water in the neutron path. Therefore, the detector located opposite to the neutron source should measure more uncollided neutrons and the neutron count rate should be higher. This can be happened in the case that not only a number of the transmitted fast neutrons can contribute to neutron count rate but also a number of forward-scattered thermal neutrons. Since as the void fraction of the nitrogen-water mixture in the test section decreased, the number of transmitted fast neutron decreased but the number of forward-scattered thermal neutron increased. Therefore, the forward-scattered thermal neutron can affect the neutron count rate of fast neutron transmission techniques. Moreover, the ^{3}He detector was more efficiency for

measuring thermal neutrons than fast neutrons. Therefore, the signals from detector might be a result of the forward scattered neutrons instead of the fast neutrons that can pass though the test section. It can be concluded that this technique was not appropriate in this work due to the result that deviated from what was expected, even though it gave a good response between the void fraction and the neutron count rate.
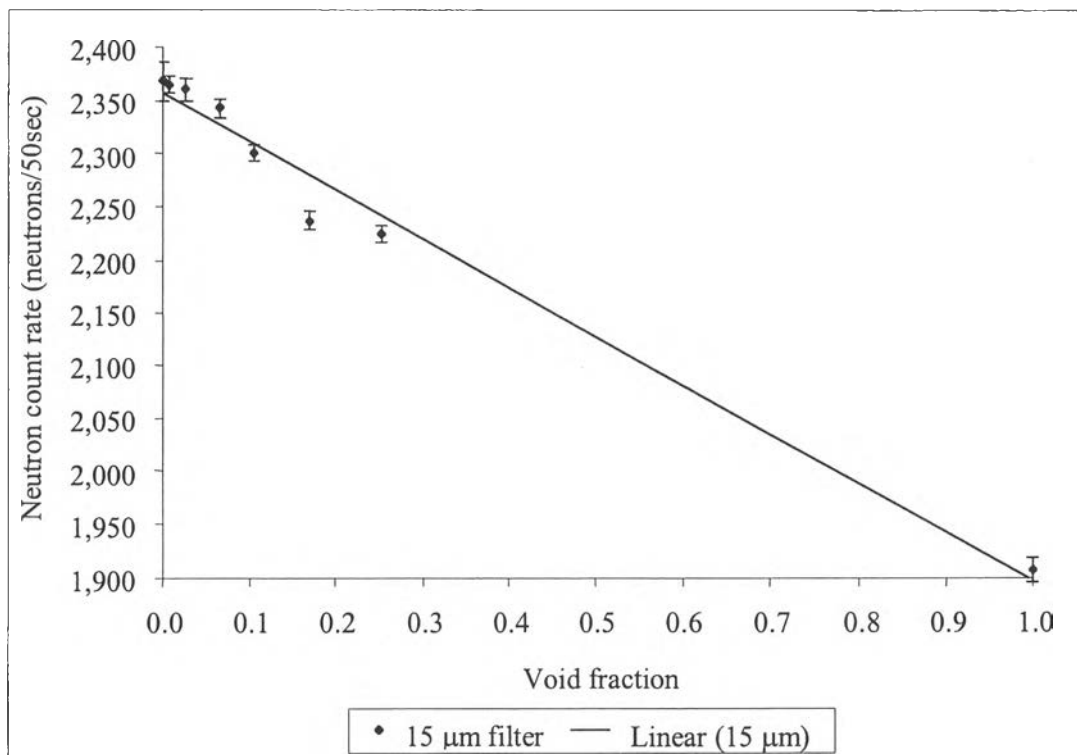
Figure 4.6 Correlation between neutron count rate and void fraction for the fast neutron transmission technique at atmospheric conditions.

However, decreasing the detector aperture can reduce the number of scattered neutron seen by the detector. The easiest way was by increasing the distance between the detector and the test section.

4.4 Dynamic Steam-Water Experiment

The dynamic steam-water experiment focused only on the fast neutron scattering technique and developed the scatterometer for on-line steam quality measurement.

4.4.1 Study of Temperature Effects

Table 4.2 shows the neutron count rate for the counting period of 10 seconds at different density values, which were obtained from the steam tables (Smith *et al.*, 1996). The raw data are found in Appendix F.2. The correlation between the density of compressed liquid and the count rate in Figure 4.7 indicated that at constant pressure, when the temperature decreased, the neutron count rate increased presumably due to the increase in the density of the water.

Table 4.2 Count rate for 10 seconds at different density values.

Density of compressed water (lbm/ft^3)	Neutron count rate (neutrons/10sec)
61.71	90019
60.74	89329
59.89	88314
57.41	86913
54.19	85441

The probability of neutron interaction was higher at a higher density because of the larger number of hydrogen atoms per unit volume. It can be concluded that temperature did have an affect the neutron count rate. As temperature decreased, the neutron count rate also increased. However, the departure from linearity in Figure 4.7 may be due to the efficiency of detector for measuring different neutron energies.
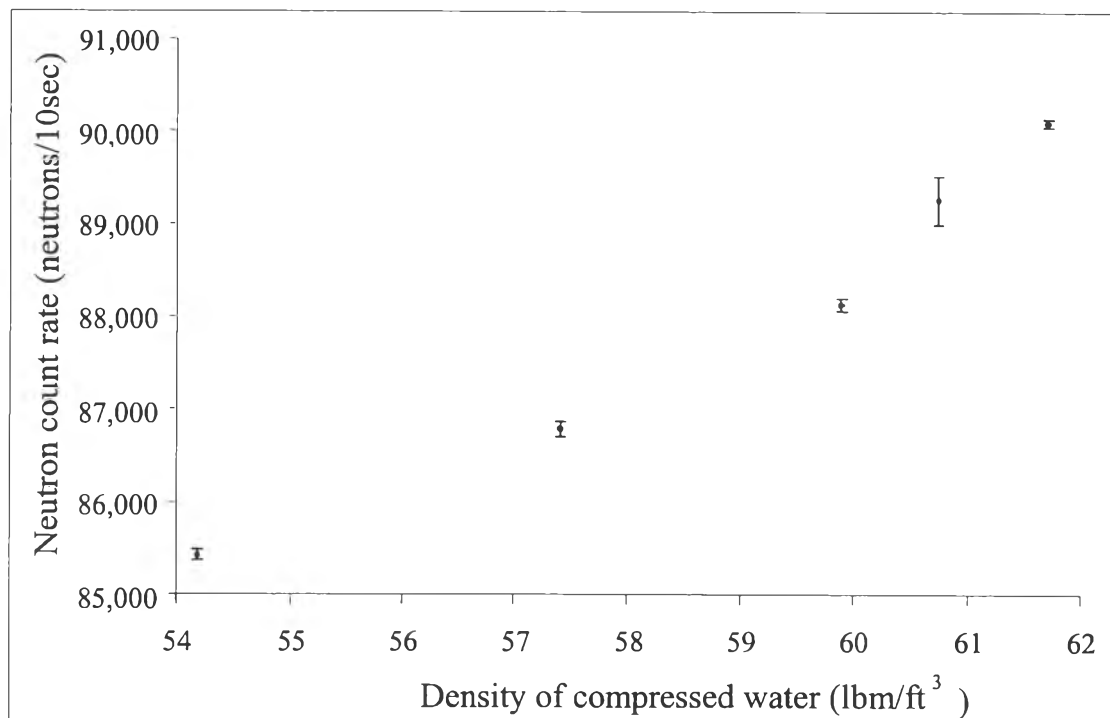
Figure 4.7 Correlation between neutron count rate and density of compressed water at a pressure of 5 MPa and different temperatures.

4.4.2 Steam Quality Measurements

Steam quality was changed by altering the setting of the autoclave heater and was calculated from thermodynamic parameters. The typical steam quality calculation was shown in Appendix. G. All results are shown in Table 4.3 and the raw data is in Appendix F.2. The experiments were performed at three different saturated conditions by varying the temperature from 150°C to 250°C.

Table 4.3 Dynamic steam-water experiment for different saturated conditions.

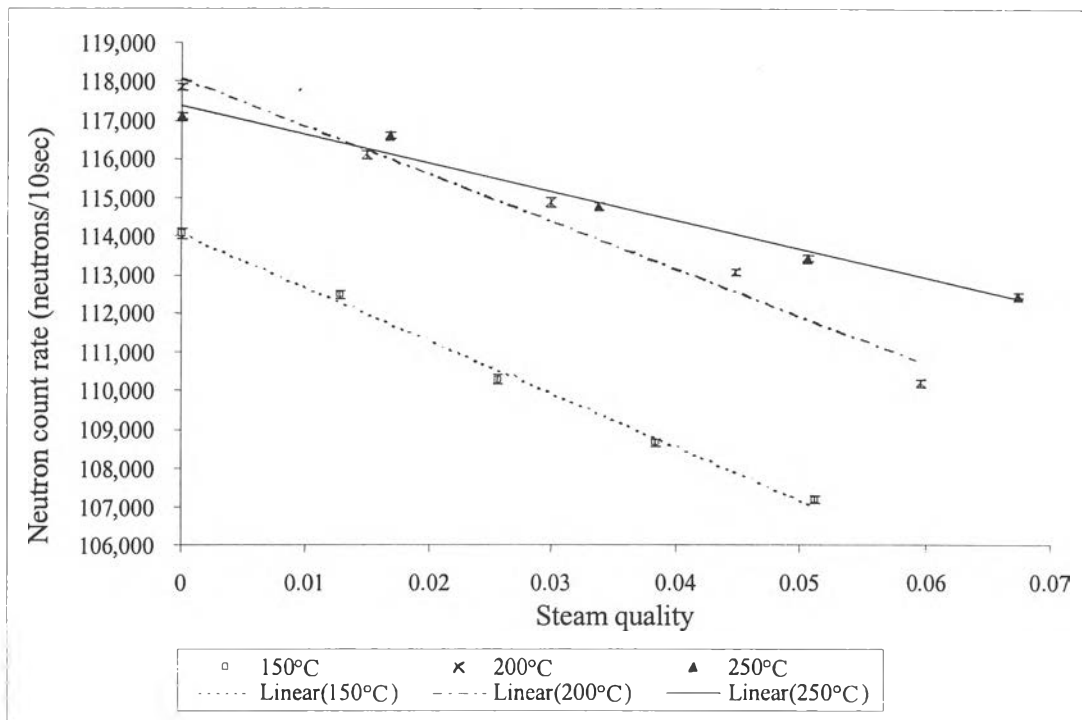| % Power of heater	150°C		200°C		250°C	
	Steam quality	Count rate	Steam quality	Count rate	Steam quality	Count rate
100%	0.0512	107187	0.0596	110184	0.0674	112445
75%	0.0384	108652	0.0447	113086	0.0506	113419
50%	0.0256	110280	0.0298	114868	0.0337	114773
25%	0.0128	112485	0.0149	116116	0.0169	116616
0%	0	114075	0	117863	0	117117

Figure 4.8 Comparison of the correlations between neutron count rate and steam quality for three different temperatures.

Figure 4.8 shows that the neutron scatterometer can be used to detect steam quality for each saturated condition, since a linear response between the neutron count rate and steam quality was achieved in all cases. The slopes of the

correlations for 150°C and 200°C were parallel. This meant that the scatterometer can be used at temperature in the range from 150°C to 200°C with the average calibration curve. It should give the same response between the neutron count rate and steam quality. However, the slope at 250°C was different, suggesting that different calibration curve was required at temperatures above 200°C. The different shallower curve may be due to the fact that at the higher temperature the difference in density between steam and water was less or was suggested later experimental error. The measurements were repeated for each temperature, as shown in Figures 4.9-4.11, in order to confirm the reproducibility of the data by comparing the slopes of equivalent data series as shown in Table 4.4. It was shown that the differences between two data series of each temperature were in the range from 25 to 35%. This was probably from the experimental errors such as the change in system geometry due to the expansion of the test section at the higher temperatures.

Table 4.4 Comparison of slopes of repeatable data series at three different temperatures.

Temperature(°C)	Slope of data series No.1	Slope of data series No.2	%difference
150	102318	137584	25.63
200	89806	123346	27.19
250	74379	50239	32.46

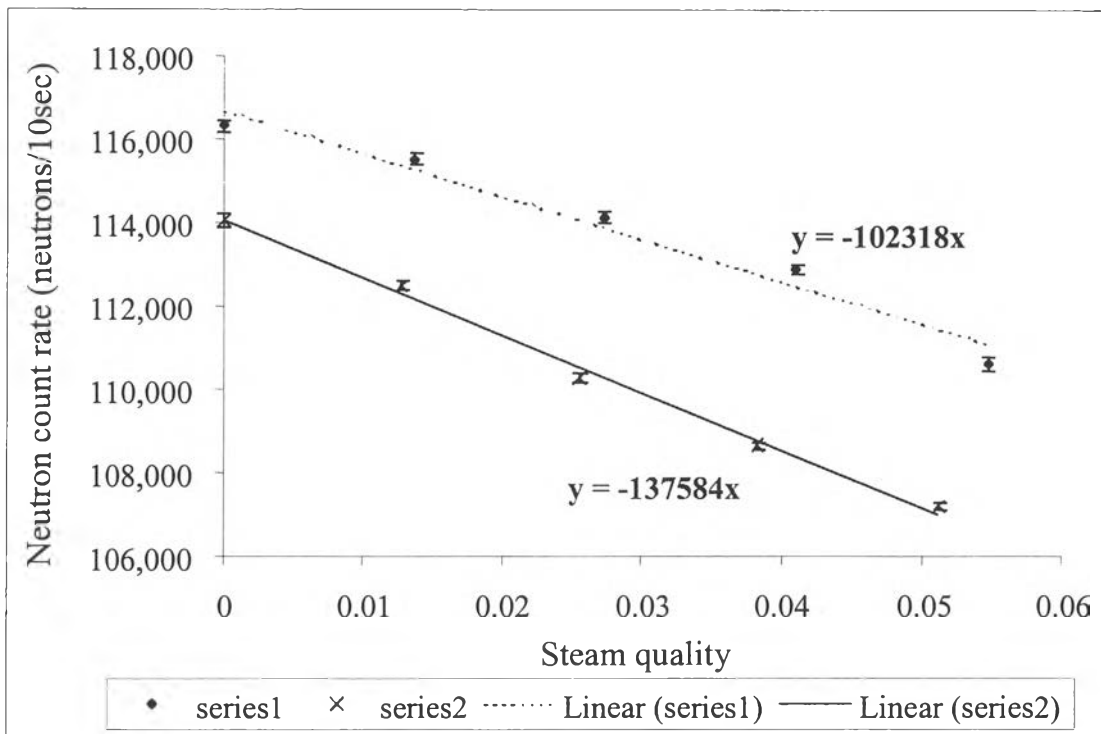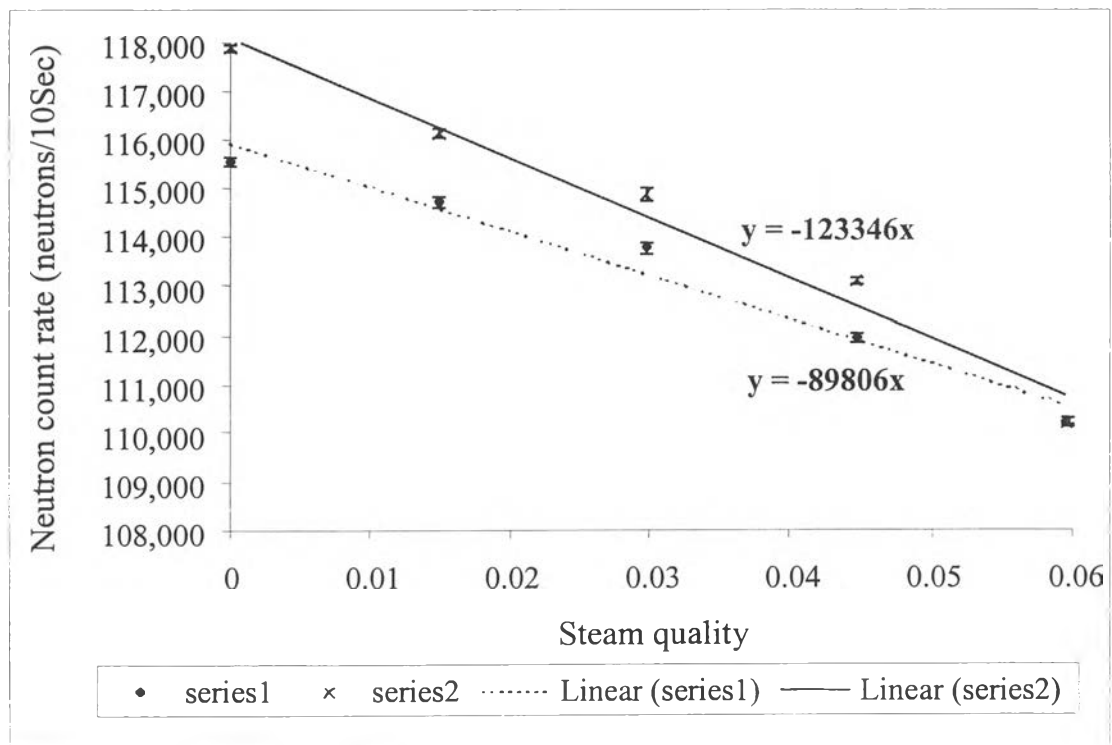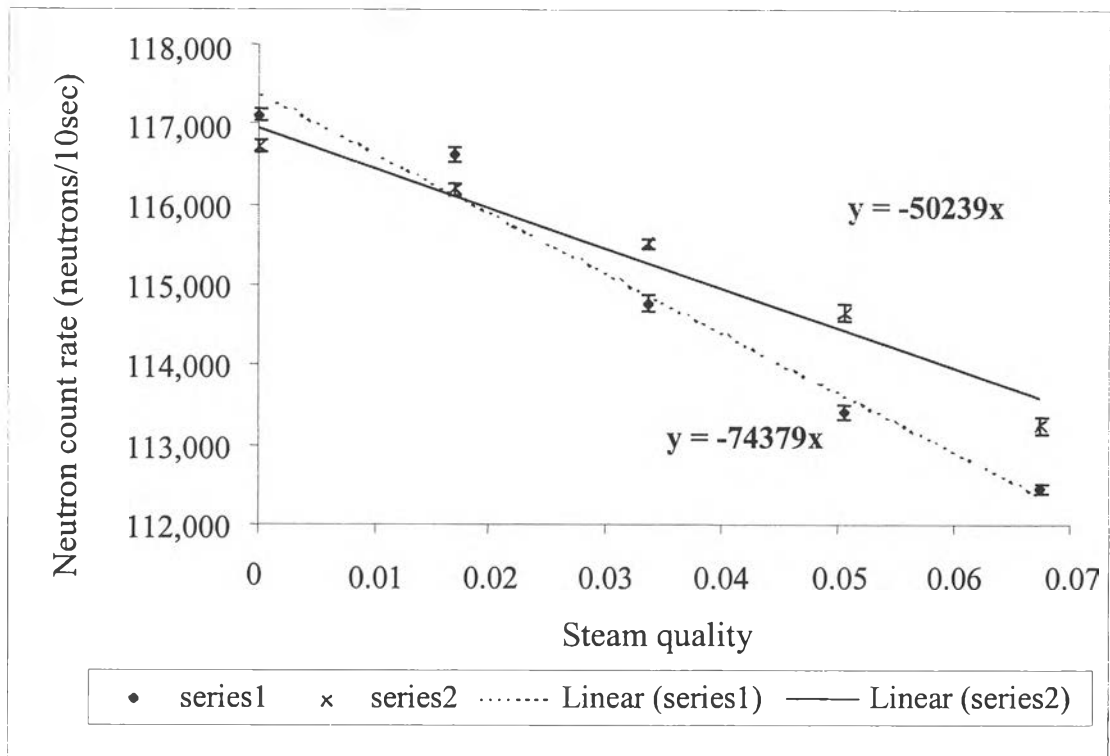**Figure 4.9** Two series of repeatable data at 150°C.

Figure 4.10 Two series of repeatable data at 200°C

Figure 4.11 Two series of repeatable data at 250°C.